ON PNT INTEGRITY IN SNAPSHOT AND RECURSIVE POSITIONING ALGORITHMS FOR MARITIME APPLICATIONS

Luís Lança, Michailas Romanovas, Ralf Ziebold

German Aerospace Centre (DLR)
Institute of Communications and Navigation
Kalkhorstweg 53, 17235, Neustrelitz, Germany
Email:{Luis.Lanca, Michailas.Romanovas, Ralf.Ziebold}@dlr.de

Contents

1 Introduction

Within the last decades one had witnessed a rapid development of new technologies for nautical applications in order to support constantly increasing marine traffic and to improve the safety of navigation in overcrowded routes. Here the process of the vessel navigation is supported by a variety of independent sources of navigational information (sensors or sensor systems), where the Global Navigation Satellite Systems (GNSS), in particular the Global Positioning System (GPS) is often adopted as key component for provision of absolute position, velocity and precise time information (PVT). However, the GNSS is usually not integrated with other on-board already existing sensor systems (e.g. speed log, gyro compass, etc.). Therefore, with the variety of independent sources of navigational information available, the process of navigation can be formulated as a real-time decision making process that requires an extreme focus and constant attention from the navigator. In spite of all the efforts to improve the quality and reliability of separate sensors, 43% of the total number of accidents in the Baltic Sea during 2012 were actually caused by human elements such as mistakes in the planning process or skill-based errors, such as slip and lapse (HELCOM 2014).

In order to reduce the complexity of the sensor data assimilation (fusion), decision making process and to improve the overall safety of berth-to-berth navigation, the International Maritime Organization (IMO) had developed within the context of the e-Navigation (e stand for electronically enhancement) initiative a Maritime Integrated Navigation System (INS) baseline architecture concept. Here the recognized vulnerability of pure GNSS solution to harsh RF signal environments introduces concerns to the provision of on-board reliable navigational data required in maritime safety-critical applications (SCA). A critical action line of the INS strategic implementation plan (SIP) aims to improve the reliability and resilience of on-board

Positioning, Navigation and Timing (PNT) information through both the enhancement of existing sensors and via the augmentation with external sensors, i.e. with the methods of sensor fusion.

Here the integration of multiple sensors with independent error patterns highly improves the overall system resilience against GNSS channel contamination and is crucial in achieving a reliable provision of the PNT data. Therefore it could be advantageous to employ a complementary inertial or any other system that is able to backup GNSS and to provide a position with slowly degrading level of accuracy for a specified period of time while GNSS information is not available or is considered unreliable. The inertial navigation systems are able to overcome the GNSS vulnerability due their complementary noise properties, inherent independence from the surroundings. All this allows Inertial Measurement Unit (IMU) data to be integrated synergetically with the GNSS information so that the short term performance of the IMU and long term stability of the GNSS can be combined optimally within the hybrid system.

Although the snapshot (GNSS-only) integrity algorithm are well known for aerospace applications, few works have been reported on applying similar techniques for other scenarios such as ground or nautical navigation. As the integrated navigation solutions using combination of sensors with complementary noise properties (e.g. GNSS and inertial) are becoming more and more popular for non-aerospace applications, mainly due to appearance of relatively cheap inertial sensors of tactical grade, odometer measurements and Doppler velocity measurements, more advanced techniques for integrity monitoring in Recursive Bayesian Estimation (RBE) methods become necessary. Although some works have been reported for aerospace applications, extremely few attention has been devoted in applying similar concepts to other SCAs such as vessel navigation and the performance of these algorithms has not been confirmed in real operational conditions.

The presented work tries to close this gap to introducing the discussion on performance of the Fault Detection and Exclusion (FDE) methods for both snapshot and RBE positioning algorithms in marine applications. In order to assess the performance of the proposed techniques for hybrid navigation we employ either pure GNSS or classical hybrid inertial/GNSS system which allow the results to be easily extrapolated to other applications such as automotive and outdoor robotics scenarios. Furthermore, the obtained results are based on real operational conditions including the GNSS unmodelled effects and errors in inertial sensors such as misalignment and scale factor errors. The performance of the developed techniques is assessed in terms of the horizontal positioning accuracy and the results are evaluated with respect to the quality of the inertial sensors and adaptive GNSS measurement models.

The report concentrates on the analysis of least-squares residuals (LSR) and Kalman filter innovation (KFI) based FDE algorithms performance. This analysis consists of two parts, firstly we compare the performance of a LSR with a non-inertial Extended KFI approach for both non-weighted and weighted range error models. For this purpose of the work the GNSS fault simulator based on Monte Carlo methods was developed which is capable of adding in

a controlled manner faults to code raw measurements recorded previously during typical maritime operational scenarios (e.g. port operation). Secondly, the performance of an Error-State Extended tightly-coupled (TC) IMU/GNSS KFI algorithm is tested during a single run with data collected during coastal approach operation. Here a MicroElectroMechanical system (MEMS) gyros and fiber-optic gyroscopes (FOG) based tactical grade IMUs are used in order to assess the impact of different IMU technology on the FDE performance.

The rest of the paper is organized as follows. In Section 2 a brief discussion is provided on state of the art methods in integrity monitoring both in snapshot and recursive positioning methods. The details on relevant mathematical methods are provided in Section 3 with the description of the system setup presented in Section 4. The experimental results are shown in Section 5 with the summary and the outlook for the future research provided in Section 6.

2 Current Research Status

The Snapshot LSR Receiver Autonomous Integrity Monitoring (RAIM) developed by the civil aviation community (Parkinson et al. 1988) or the statistical reliability testing developed by the geodetic community (Teunissen 1998) are the classic references for non-augmented GPS-based LSR algorithms. All approaches make use of measurements redundancy to check, on a measurement-by-measurement basis, the relative consistency among estimated residuals in order to detect the most likely measurement fault. Most of the previously referred approaches are based on the comparison between a test statistic depending on the estimated least-squares (LS) residuals and a given threshold. The decision threshold is set considering *a priori* knowledge of the statistical distribution of the test in the fault free case and a given false detection rate. Although the classical methods mainly use snapshot techniques, some works have been reported on introducing the FDE algorithms for RBE techniques (Petovello 2002), usually formulated in a well-known form of the Kalman filter (KF), where it has been proven that the KF innovations follow the same statistical distribution as the LS residuals (Wang 2008).

A constant measurement noise assumption is often violated in real world scenarios and several approaches have been reported on increasing the robustness of the integrated solutions by considering adaptive GNSS noise models. Although it has been widely agreed that the number and the impact of the possible error sources is strongly related with the satellite elevation, but the elevation angle itself is not necessarily the best indicator of the actual signal quality. Here the CNo, which is the ratio of the received carrier (i.e. the signal) power to noise density, is often considered as a fairly good indicator of the signal quality. The measurements with higher CNo values are good indicators of less noisy range measurements and therefore are able to provide a more precise positioning solution (Wieser et al. 2000).

Augmentation of the GNSS with inertial sensors in order to mitigate intentional or unintentional RF signal interference has a fairly long history. The work of Lee et al. 2000 addressed

both the issues of IM in a TC IMU/GPS system and the availability of the hybrid navigation solution. The latter one is defined as the ability of the system to coast upon the loss of all GPS signals while still maintaining a certain accuracy. The authors in Lee et al. 2000 used GNSS ramp error model and the results indicated that both solution separation method and the extrapolation method may not detect the satellite failures during periods of low (fewer than four) satellite visibility. The authors conclude that innovations can be only used to detect the failures causing a relatively fast growing errors, while the statistics for the extrapolation method which averages the innovation vector elements over time has to be used to detect a slower error ramp. Although the MEMS sensors have attracted an increasing attention for the pedestrian localization (Foxlin 2005), certain automotive applications or low-cost UAV (Unmanned Aerial Vehicle) design, their applicability to SCA such as maritime navigation has been till recent limited by their relatively high noise and bias instability, causing a rapid drift of the standalone inertial solution when neither of the alternative reference position information is available. Some recent works (Moore et al. 2008) have also assessed a possibility to replace the FOG with higher performance MEMS IMUs and have confirmed that a combined IMU/GNSS system is able to deliver the position and the velocity information at rapid update rate while preserving a low noise content due to smoothing performance of the inertial integration, the performance of the hybrid system was not assessed under the presence of GNSS faults and no IM algorithms were evaluated.

3 Mathematical Development

The algorithms employed in maritime SCA must meet stringent reliability requirements. One of these reliability requirements is called an integrity risk (or only integrity for short) which is defined as likelihood of an undetected navigation state error that results in Hazardously Misleading Information (HMI). In practice, it is defined a confidence bound for the navigation system state which confines all the state output errors with a confidence equal or higher than 1-α, where α is the integrity risk (adjusted to the target application). There is a case of loss of integrity when the navigation system state error exceeds the confidence bound without warning the system user. The probability of loss of integrity is also called probability of HMI. This probability can be mapped onto the state space and, in the case of Kalman Filter (KF) based navigation system, can be interpreted as the protection level (in physical units) of the state uncertainty ellipsoid. The Integrity Monitoring (IM) algorithms must provide functionality for detection of the state error and exclusion of the faulty sensor from the navigation system state estimation (the so called FDE functionality) and optionally calculate the corresponding protection levels.

The algorithms for positioning and hybrid navigation are usually formulated as state estimation problems using a combination of the measurements from multiple sensors with com-

plementary noise properties. A desired set of the parameters to be estimated from the noisy measurements usually includes the pose (the object's position, velocity and attitude) as well as some of the sensor errors. Here one can utilize a well-established estimation strategy based on the RBE framework, while a classical LS solution can be considered as a non-recursive memory-less(snapshot) approach. The classical RBE cycle is performed in two steps:

Prediction The *a priori* probability is calculated from the last *a posteriori* probability using probabilistic process model f.

Correction The *a posteriori* probability is calculated from the *a priori* probability using probabilistic measurement model and the current measurement h.

In practice, however, the theoretical methods formulated with probability densities do not scale up very well and can quickly become intractable even for the estimation problems of reasonable dimensionality. Various implementations of RBE algorithms differ in the way the probabilities are represented and transformed in the process and measurement models (Thrun et al. 2005; Grewal et al. 2001). If the models are linear and the probabilities are Gaussian, the linear KF is an efficient and optimal solution of the estimation problem. Unfortunately, most of the real-world navigation systems are rather nonlinear and modifications to the linear KF have been developed to deal with nonlinear models.

The Extended Kalman Filter (EKF) is one of the most popular nonlinear estimators and is historically considered as a standard within the engineering community. In EKF the nonlinear models are linearized about the current estimate using the Taylor series expansion, where the state transition model f and observation model h are replaced by the corresponding Jacobians F and H. The system at every time t_k is represented by the state x_k and an associated covariance P_k with the rest of the filtering scheme being essentially identical to that of the classical linear KF. Although the EKF inherits many advantages of the KF such as limited computational costs and clear filtering structure, it still suffers from two main problems. Firstly, the performance of the estimator strongly depends on the validity of the linearized model assumption and can become inaccurate and lead to filter instabilities if these assumptions are violated. Secondly, the required Jacobians can be potentially difficult or even impossible to derive if dynamical models involves complex approximation coefficients and/or discontinuities.

The usual GNSS-based position determination involves four unknowns: receiver coordinates (X, Y, Z) and the receiver clock offset δt ($n = 4$). For the memoryless least-squares (LS) estimation we follow a classical approach with linearization of the measurement function at each epoch t_k around a point x_0 and finding the correction factor $\delta\hat{x}$ using (Borre et al. 2010):

$$\delta\hat{x} = \left(H^T R^{-1} H\right)^{-1} H^T R^{-1} \delta z, \tag{1}$$

and the iterative update of the initial estimates $x_i = x_{i-1} + \delta\hat{x}_i$, where δz is the misclosure vector and R is the measurement noise covariance. If there are five or more observations z available (i.e. $m > n$), the redundant measurements could be used to check the consistency among the

full set of the measurements. This forms a fundamental principle for the fault detection using LS method, where the measurement space with dimensionality m is separated into two subspaces: the state space and the parity space with the dimensionality n and $m-n$ respectively (Joerger et al. 2010). The LSR methods are based on the detection test derived from the measurement residual norm $\|e\|$:

$$\hat{e} = z - H\hat{x} = (I - H(H^T R^{-1} H)^{-1} H^T R^{-1}) z. \tag{2}$$

The test statistics is based on the estimated residual vector $\|\hat{e}\|^2$ normalized by the standard deviation of the measurement errors $\|\hat{e}\|^2 = \hat{e}^T R^{-1} \hat{e}$, and R is the measurement noise covariance.

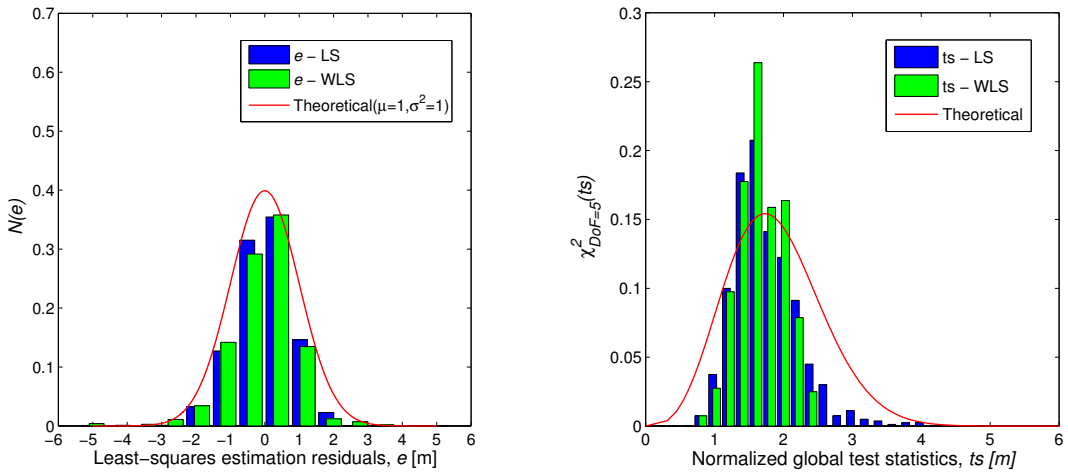

Figure 1: Least-squares estimation residuals probability density function (left) and the normalized global test statistics probability density function (right).

This statistics is observable whereas the positioning error of the LS solution is not. In the fault-free case (the individual residuals follow $\mathcal{N}(0,1)$, see Fig.1 (left), the value follows a central Chi-Square distribution with $m-n$ degrees of freedom and expectation equal to zero (see Fig. 1 (right)). Here the classical LS detection method is based on the hypothesis testing which compares the test statistics with the given threshold. The weighted LS RAIM statisticsis defined as follows $ts = \sqrt{\|\hat{e}\|^2}$ (Walter et al. 1995).

Under the assumption of fault-free case, the test threshold Th for a given probability of false alarm (Pfa) and redundancy (or equivalently, degrees of freedom) is found by inverting the incomplete gamma function (Walter et al. 1995). A common procedure consists of fixing Pfa according to the application requirements and letting the threshold vary with the measurement redundancy. A typical value for Pfa in maritime applications is 0.1% (Ryan 2002). The hypothesis test is given by the following condition:

$$\text{Global-Hypothesis-Test} = \begin{cases} H_0 & \text{if } t_s \leq T_h, \\ H_1 & \text{if } t_s > T_h. \end{cases} \tag{3}$$

This test can be seen as a global one as it checks the consistency of full measurement set. The threshold determines whether the null-hypothesis of the global test is accepted or rejected. If it is rejected, an inconsistency in the tested measurements is assumed and the fault source should be identified and further excluded using, e.g, the local test (Kuusniemi 2005; Petovello 2002). This test assesses the standardized residuals defined as follows:

$$r_i = \left| \frac{\hat{e}_i}{\sqrt{U_{i,i}}} \right|, i = [1, \ldots, n], \tag{4}$$

where U is the covariance matrix for residuals $U = R - H(H^T R^{-1} H)^{-1} H^T$.

In order to detect a fault, each standardized residual r_i is tested using the quantile of a normal distribution equal to the Pfa. In the local test, the residual under test is excluded if the respective standardized residual exceeds the test threshold. Similarly to the global test, the local test assumes the residuals to follow $\mathcal{N}(0, 1)$. The local hypothesis test is given by the following condition:

$$\text{Local-Hypothesis-Test} = \begin{cases} H_{0,i} & \text{if } r_i \leq Q_{(1-Pfa/2)} \\ H_{1,i} & \text{if } r_i > Q_{(1-Pfa/2)} \end{cases} \tag{5}$$

where Q_p is the quantile of the probability p of the standard normal distribution. Only the measurement with a large r_i is tested against the $H_{0,i}$, as a measurement fault affects multiple standardized residuals. The measurement *i* is selected as a candidate to be excluded if and only if both the following conditions are fulfilled:

$$\begin{cases} r_k \geq r_i, \ \forall i \\ r_k > Q_{(1-Pfa/2)} \end{cases} \tag{6}$$

The approach for RBE algorithm (in our case represented by EKF) is rather similar to the one for the snapshot algorithm. The predicted residual vector (some times called innovation vector) is given as follows:

$$d_k = z_k - h(x_k), \tag{7}$$

where $h(x_k)$ is a non-linear function relating the states to the observations. The innovation vector can be considered as an indication of the amount of information introduced in the system by the actual measurements and the respective normalized norm can be used again as the measurement quality indicator. For a fault-free situation, this norm follows a central Chi-Squared distribution with m degrees of freedom with the global test statistics given by $ts_{KF} = \sqrt{\hat{d}_k^{\ T} S_k^{-1} \hat{d}_k}$. Here S_k is the innovation vector covariance matrix defined as $S_k = H_k P_k^- H_k^T + R_k$. The global test and the local tests are performed following the same procedure as for the LS methods described before. Again it is assumed, under fault-free conditions, the innovations to be zero mean Gaussians.

The FDE scheme implemented in this work consists of a two-step procedure based on the

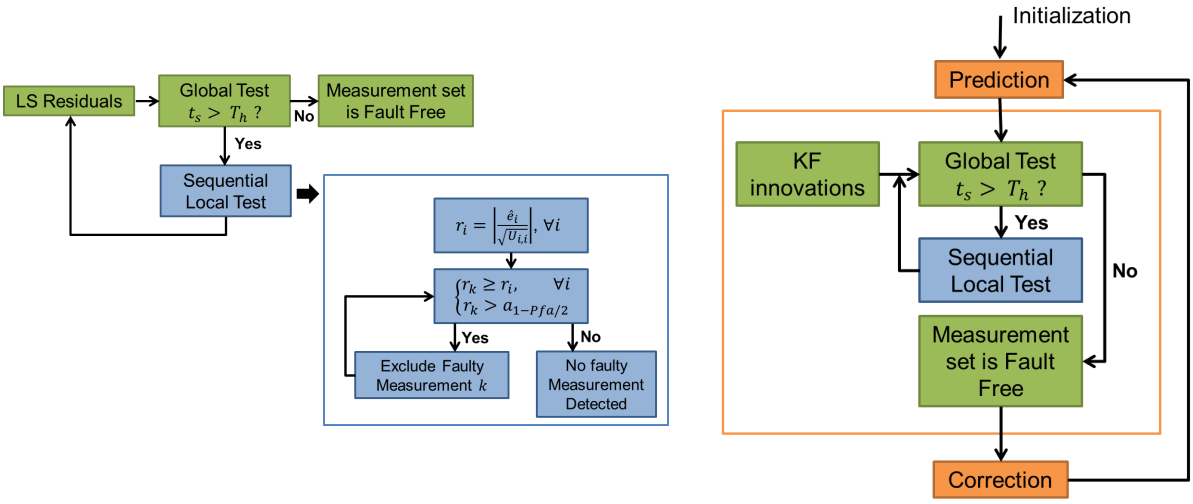

Figure 2: Two-step FDE test procedure scheme: LS residuals (left) and KF innovations (right).

global and local test as shown in Fig. 2. Firstly, the global test, as described before, checks the consistency among the full set of measurements. In the case some inconsistency is detected, the scheme performs a local test. The local test is recursively applied whenever a fault is detected until no more faults are found (Kuusniemi 2005). According to (Diesel et al. 1995) the innovation property makes it possible to detect very slow satellite drifts by estimating the mean of the residuals over a long time interval, where in order to avoid contamination of the KF estimated state, the measurements and residuals are stored in buffers for periods up to 30 minutes.

As the basis for the adaptive pseudorange measurement noise covariance model σ^2 we have adopted the following expression:

$$\sigma^2 = a + b \cdot 10^{-\frac{CNo-c}{10}}, \tag{8}$$

with three approximation parameters a, b and c. Here the parameter a can be roughly mapped to the receiver correlator noise baseline. In the expressions above the CNo is the measured carrier to noise density ratio for a particular pseudorange observation. The resultant model along with the experimental data are shown in 3.

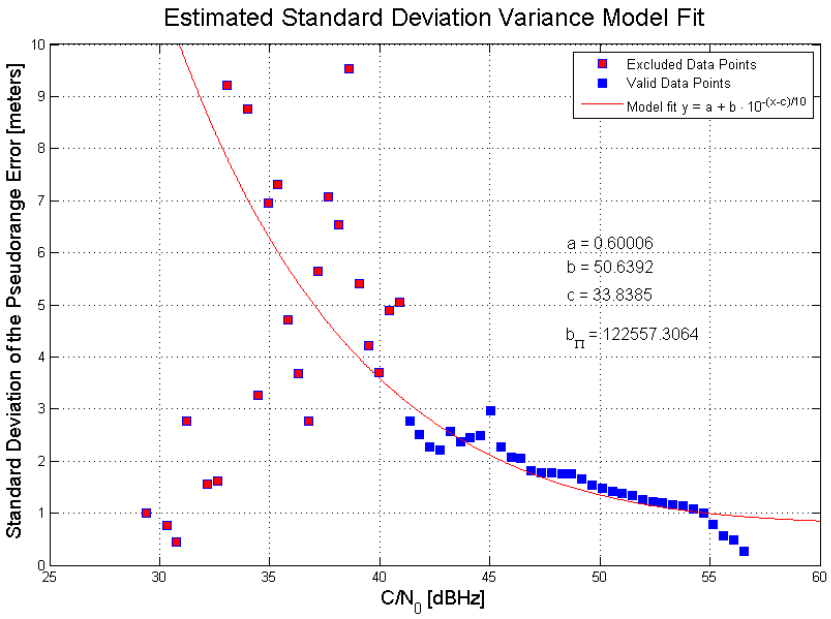

Figure 3: Experimental data for pseudorange noise model and model fit results. Only valid data points were employed for the noise model extraction.

4 System Setup

In order to overcome the previously identified issues and to commit with the IMO SIP, the DLR has developed a PNT unit concept (Ziebold et al. 2010) and an operational prototype in order to confirm the unit performance under real operational conditions. Here the core goals are the provision of redundancy by support of all onboard PNT relevant sensor data including Differential GNSS (DGNSS) and future backup systems (e.g., eLoran), the design and implementation of parallel processing chains (single-sensor and multi-sensor architectures) for robust PNT data provision and the development of the IM algorithms to evaluate the events or conditions that have the potential to cause or to contribute to HMI and could compromise safety.

The experimental setup for our PNT Unit developments is described as shown in Fig. 7. The original sensor measurements were recorded using the multipurpose research and diving vessel Baltic Diver II (length 29 m, beam 6.7 m and draught 2.8 m, GT 146 t) as a base platform for the PNT unit development for nautical applications at DLR. The vessel was equipped with three dual frequency GNSS antennas and receivers (Javad Delta), FOG and MEMS IMUs, gyrocompass, Doppler speed log and echo sounder. The IALA (International Association of Marine Aids to Navigation and Lighthouse Authorities) beacon antenna and receiver were employed for the reception of the DGNSS code based corrections. The VHF modem was configured for the reception of the RTK (Real-Time Kinematics) phase based corrections data from our Maritime Ground Based Augmentation System (MGBAS) station located in the port of Rostock (Minkwitz et al. 2010; Noack et al. 2009). All the relevant sensor measurements are provided

either directly via Ethernet or via serial to Ethernet adapter to a Box PC where the observations are processed in real-time and stored in a SQlite3 database along with the corresponding time stamps. The described setup enables a record and replay functionality for further processing of the original sensor data. The system consists of a highly modular hardware platform and Real-Time software Framework (RTF) implemented in ANSI-C++.

Figure 4: The PNT unit prototype in laboratory conditions.

The data were recorded on the 01/09/2014 in a quasi-static scenario where the vessel was moored at its home port Alter Fischereihafen on the river Warnow close to the Rostock port. At this time there was only weak wind and little waves, so that only minor vessel motion could be observed. The evaluation is based on data from the mid ship antenna, which is located besides the main mast of the ship and some shadowing effects are still expected. The chosen environment represents a typical maritime port application. The dynamic data used to test the IMU/GNSS integrated system was collected using the same setup and vessel during a coastal approach operation.

For the purpose of the work the GNSS fault simulator based on Monte Carlo methods was developed which is capable of adding in a controlled manner faults both to code and Doppler raw measurements recorded previously during typical maritime operational scenarios (e.g. port operation). The simulator allows selecting static and dynamic faults profiles, such as stepwise and ramp fault signatures. Stepwise faults simulate the measurements additive faults (e.g. signal multipath) and ramp faults correspond to slowly-varying accumulative errors (e.g. satellite clock drift). The simulated fault profile, amplitude range and fault duration time is configurable for a single satellite at the time. As the fault impact on the estimated state is strongly influenced by the satellite geometry, the fault onset time is randomly selected within the period the satellite is visible. The raw data selected for the simulation are assumed to be fault free to avoid misdetections. In order to make the analysis statistically significant, a large number or runs was performed to cover an extended fault amplitude range and different visible satellites. For all runs the same raw data is used while the satellite vehicle ID, fault onset time and amplitude are allowed to vary.

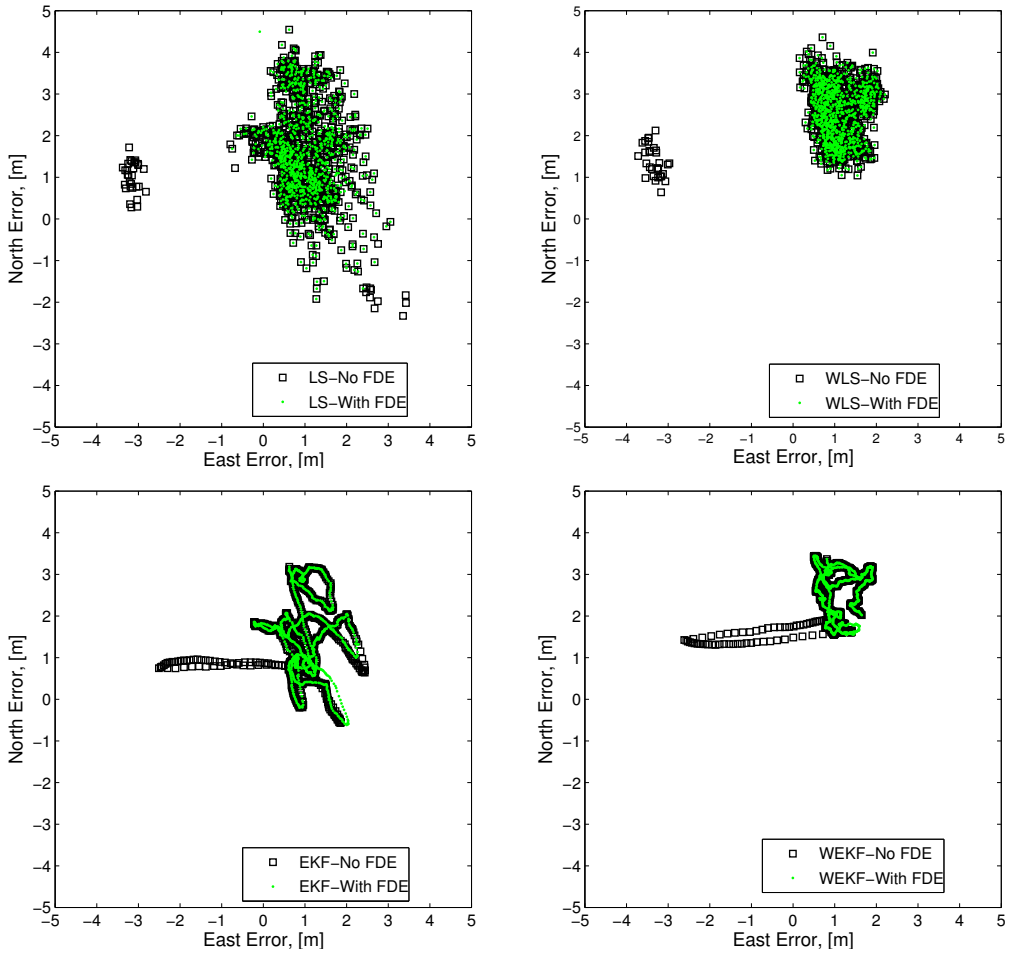

Figure 5: Precision of the approaches with and without FDE scheme: LS with constant noise model (top-left), LS with weighted noise model (top-right), EKF with constant noise model (bottom-left) and EKF with weighted noise model (bottom-right).

5 Results

In order to evaluate the performance of the methods, a realistic adaptive pseudorange noise model was extracted. The experimental data have been obtained from a reference receiver of known position over 24 hours using broadcast ionospheric and tropospheric corrections with the error statistics computed by analyzing the differences between the expected and the observed ranges. The obtained data have been binned according to the associated CNo values and for each bin a variance was estimated. Note that in this simplified approach only variance was modeled as a function of the signal quality and the non-zero mean offset was ignored. Figure 3 shows the experimental results and the extracted model using a nonlinear least squares fit. The points with lower CNo values have been manually excluded as having insufficient statistics and fit was found only to the values larger than 40 dB-Hz. Moreover, the performance of the DLL (Delay Lock Loop) correlator in the GNSS receiver to track the satellite pseudoranges is often poor for low CNo values and the obtained values are simply not representative. The

extracted model was used in weighted methods as described below and allows construction of both adaptive LS and KF schemes.

Note that the experimental data show also a small noise for CNo larger than 55 dB-Hz. The observed values are close or even smaller than the correlator base noise level and are probably caused by the insufficient sample size for larger CNo values. Still this effect has been effectively eliminated from the fit model as the parameter a is almost 60 cm which is close to the rough theoretical calculations for the associated hardware. This also allows us not to exclude these points manually as both LS and KF algorithms have shown relatively low sensitivity to a small variations in variance models.

Figure 5 shows the results of the implemented FDE on accuracy of a classical LS solution with constant (top-left) and weighted (top-right) measurement noise models with the corresponding results for the EKF shown in (bottom-left) and (bottom-right) in the presence of an artificially generated step fault of 15 meters. Clearly, the proposed FDE mechanism is able to detect and eliminate the fault. As expected, the overall precision is improved when using an adaptive measurement model, although a slight shift in the mean position can be seen. The latter effect can be explained by a slight mismatch of the constant and adaptive noise models in terms of an overall impact with respect to assumed noise dynamics as well as a particular satellite geometry. The provided figures are generated by converting the solver solution (X, Y, Z) coordinates to ENU (east-north-up) frame and centering them with respect to the RTK mean position which corresponds to the coordinates (0,0) in Fig. 5. As we have seen in Fig.5, the adaptive noise approach significantly improves the spread of the solution around the mean, although the effect of a slight shift of the mean position still needs some further investigation.

The FDE exclusion rate statistics is shown in Fig. 6 both for weighted and non-weighted LS and KF methods. In all the non-weighted approaches the $\sigma = 2$ meters was used which is reasonably close to the average residual value of 2.3 meters extracted from reference data employed for adaptive model calculation. Clearly, for reasonably large fault amplitudes all the methods converge to the detection rate of 100%, although the performance for moderate fault amplitudes is significantly different. Although the shown results confirm a superiority of the KF-based FDE scheme over a snapshot LS approach, the provided results represent an averaged behavior and the impact of the particular satellite is not clearly visible as the performance statistics for a particular satellite could be different from the shown averaged behavior depending on the geometry and associated CNo values. Due to a short duration of the test scenario we were not able to sample different satellite geometries and should be investigated in future.

The results from above confirm that the FDE KF-based techniques constantly outperform the non-KF techniques when equivalent measurement noise model is used. This, however, should come at no surprise as the KF has an explicit dynamics model (in this case a static position model is assumed for non-inertial approach) which fits nicely to the scenario and the results could be worse when the KF process model does not match the true dynamics. This is, fortunately, not a problem for the system in mind when the inertial sensors are employed within the

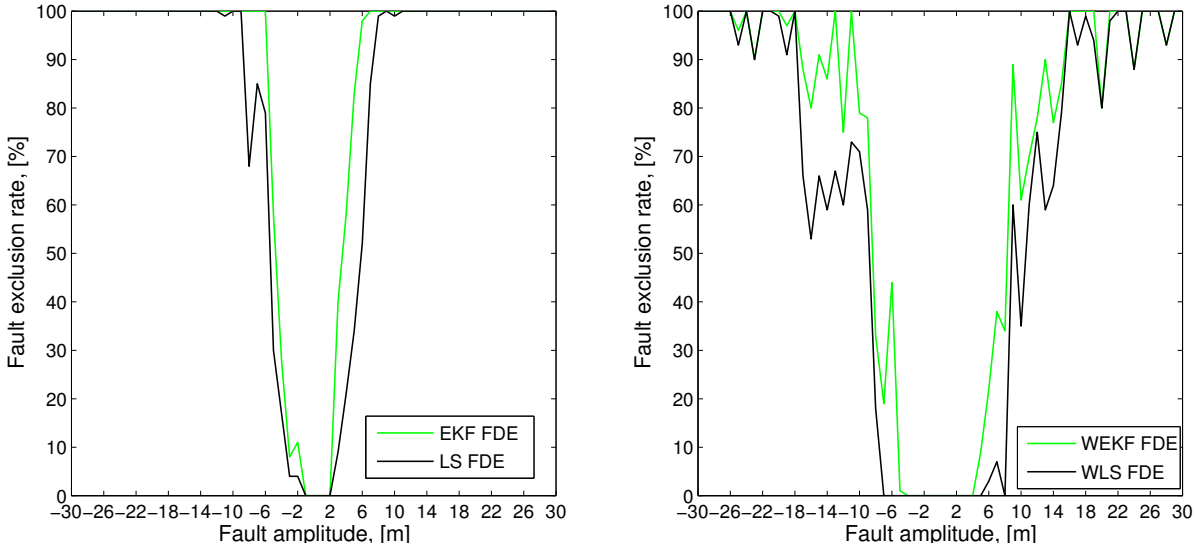

Figure 6: Fault exclusion rate in Monte-Carlo simulation. The non-weighted LS and KF approach (left) and the weighted LS and KF methods (right). In both cases the elevation mask of 8° was applied and $Pfa = 0.001$ was used.

prediction step. In this case the process dynamics is based not on the assumptions on expected motion models, but rather on a true dynamics provided by a direct strapdown integration. The inertial unit provides a true short-term stable dynamics and the FDE mechanism benefits from this information.

For the weighted noise model the fault exclusion rate is extremely noisy and converges to 100% only for the fault amplitudes close to 30 meters. This, however, is a direct result of the adaptive noise model which assigns increased measurement noise variance for satellite signals with low CNo values and could lead to the situations where even the faults of significant amplitudes can be still considered 'within' the measurement statistics of the satellite with bad CNo and therefore are not excluded. Here comes an important conclusion that a direct adoption of the weighted measurement model, although results in accuracy improvement, could also lead to the failure of the FDE or similar mechanisms. Thus, both adaptive noise model and FDE scheme seem to be mutually exclusive strategies: while the FDE scheme tries to check the measurement consistency using given statistics and eliminate the observations which violate correct measurement assumption, the weighted approach tries to adjust the statistics to fit the observations and simply down-weighs the measurement of poor quality.

Obviously, a constant amplitude step can be hardly considered as the most representative sensor failure approach. For example, a performance of the KF-based techniques can become much worse for the ramp-like scenarios, where small amplitude and prolonged duration offsets in one of the measurements, when initially undetected, could force the filter to drift significantly from the true estimate. On the other hand, the step-like faults form a fairly representative error model when one considers multipath effects in maritime environments (Ryan 2002).

In Fig. 7(left) we can see the average impact of the amplitudes of injected faults on the

estimated state (position) within the non-inertial EKF. For comparison, the impact on the system with augmented FDE functionality is also shown. Firstly, the RBE method achieves an improved error performance compared to memory-less LS approach due to its implicit dynamic model, which is employed within the KF to predict the future position. Consistently, the performance of the KF with FDE is also better than the performance with FDE, where the KF approach results in almost 2x smaller maximum position error (note that the exact gain is a trade-off of both process and measurement noises). Moreover, the fault amplitude which corresponds to the inflection point is also smaller for the KF method compared to the LS technique and this is consistent with the earlier rise of the exclusion rate curve as shown in Fig. 6(left). The observed values can be also interpreted as HMI for the system user as the represent the maximum impact in the estimated position caused by the undetected faults in the measurements.

Finally, we evaluate the FDE performance within the TC IMU/GNSS architecture and assess the impact of the inertial sensor quality on the final accuracy of the integrated approach. Fig. 7(right) shows the horizontal position error (HPE) in the case of fault in true data (non-simulated fault) during the coastal approach. In order to distinguish between the effect of inertial smoothing and FDE, additionally the HPE of a loosely-coupled (LC) EKF (without FDE) and the least-square solution without FDE (referred as SPP in Fig. 7 (right)) are shown. Here the position and velocity of the SPP serve as direct observations instead of using separate measurement fusion in the TC architecture, and, therefore, a FDE scheme based on single satellite signals is not applicable. One sees that the smoothing behavior of both TC and LC EKF is comparable, but during the measurement fault, the LC solution slowly follows the wrong position from the SPP, whereas the FDE in the TC EKF ensures that the faulty measurements are removed from the navigation solution. A manual inspection of the faults during that 24h time span leads to the conclusion, that all of these faulty measurements are simultaneously detected by both, the TC EKF with FOG and MEMS IMU and the quality of the inertial sensor does not seem to play a significant role for the algorithm performance. Clearly, an in-depth statistical analysis is still necessary in order to confirm that also smaller GNSS faults (offsets) can be also detected using lower cost MEMS IMU.

6 Summary and Outlook

Within this preliminary work we have successfully demonstrated an application of the FDE mechanism for fault detection and exclusion both in snapshot and KF-based algorithms for maritime applications. The proposed methods form a solid foundation for construction of more reliable and robust PNT unit, where state-of-the-art hybrid navigation algorithms are augmented with integrity monitoring functionality to ensure the performance of the system during e.g. GNSS faults. The presented work is implemented within a framework of the integrated PNT unit with an additional integrity monitoring functionality. The FDE mechanism provides con-

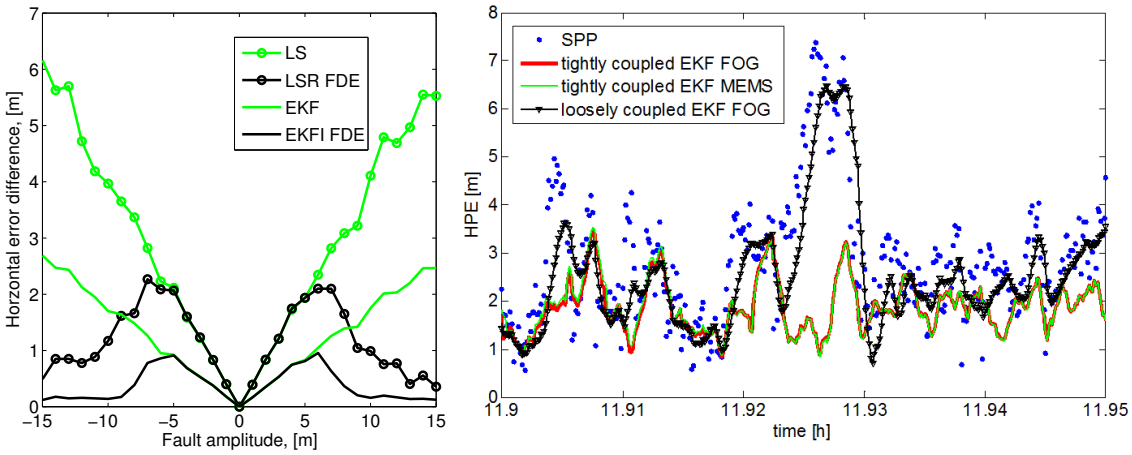

Figure 7: Effect of the injected fault amplitudes on the estimated position (left) and HPE of SPP, loosely- and tightly-coupled (with FDE) EKFs for a scenario with inherent fault (right).

sistent improvements in terms of the horizontal accuracy both in LS and RBE methods. An interesting behavior of the proposed FDE mechanism has been noticed for the methods with CNo-dependent measurement noise models, where the fault detection rate had shown worse performance compared to that of the non-adaptive methods. The performance of the proposed methods was evaluated using real measurements from the vessel combined with Monte-Carlo simulation for the fault detection. Additionally we confirm that the quality of the IMU is not critical for the FDE functionality within the TC IMU/GNSS architectures and this finding is an important step in reducing the price of the complete PNT unit. Apparently, the quality of the inertial sensor (in terms of additive noise and bias stability) is only important for bridging GNSS outages (standalone strapdown inertial mechanization) - i.e. for *contingency* functionality.

Further work is planned in extending the presented concepts for the GNSS Doppler shift measurements both in snapshot and RBE algorithms and more detailed analysis is required to assess the impact of the faults not only on the position, but also on the rest of the estimated state, including the velocity and the attitude (in IMU/GNSS integrated approaches). Correspondingly the proposed techniques have to be verified for hybrid IMU/GNSS and Doppler Velocity Log navigation systems and the performance of the associated FDE algorithms has to be confirmed for complex sensor fusion scenarios. Moreover, while implementing the proposed schemes a special attention has to be paid to a challenging problem of the memory effects in RBE schemes as the typical implementations based on Kalman filtering are, in principle, infinite memory filters. Clearly, the associated upper error bounds in estimated position, velocity and attitude have to be taken into account for the analysis to be complete. Finally, robust methods have to be developed for the decision matrix functionality, where the system switches between different channels (algorithms with different sensor combinations) using the available FDE results and corresponding channel integrity information.

7 Bibliography

Borre, Kai and Gilbert Strang (2010). *Algorithms for Global Positioning*. Wellesley-Cambridge Press. Chap. Essential Ideas And Applications of GNSS, pp. 8–11.

Diesel, John and Sherry Luu (1995). "GPS/IRS AIME: Calculation of Thresholds and Protection Radius Using Chi-Square Methods". In: *Proceedings of the 8th International Technical Meeting of the Satellite Division of The Institute of Navigation (ION GPS 1995)*. Palm Springs, CA, pp. 1959–1964.

Foxlin, E. (2005). "Pedestrian tracking with shoe-mounted inertial sensors". In: *Computer Graphics and Applications, IEEE* 25.6, pp. 38–46. ISSN: 0272-1716.

Grewal, M. S. and A. P. Andrews (2001). *Kalman Filtering. Theory and Practice using MATLAB, 2nd edition*. John Wiley & Sons, Inc. New York.

HELCOM (2014). *Annual report on shipping accidents in the Baltic Sea area during 2012*. HELCOM Baltic Marine Environment Protection Commission.

Joerger, Mathieu and Boris Pervan (2010). "Sequential Residual-Based RAIM". In: *Proceedings of the 23rd International Technical Meeting of The Satellite Division of the Institute of Navigation (ION GNSS 2010)*. OR, pp. 3167–3180.

Kuusniemi, Heidi (2005). "User-Level Reliability and Quality Monitoring in Satellite-Based Personal Navigation". PhD thesis. Tampere: Tampere University of Technology.

Lee, Young C. and Daniel G. O'Laughlin (2000). "A Performance Analysis of a Tightly Coupled GPS/Inertial System for Two Integrity Monitoring Method". In: *Navigation* 47.3, pp. 175–189. ISSN: 2161-4296.

Minkwitz, David, Stephan Schlüter, and Jamila Beckheinrich (2010). "Integrity Assessment of a Maritime Carrier Phase Based GNSS Augmentation System". In: *ION GNSS 2010*. Institute of Navigation. Portland, USA.

Moore, Terry, Chris Hill, Andy Norris, Chris Hide, David Park, and Nick Ward (2008). "The Potential Impact of GNSS/INS Integration on Maritime Navigation". In: *The Journal of Navigation* 61, 221237.

Noack, Thoralf, Evelin Engler, Anja Klisch, and David Minkwitz (2009). "Integrity concepts for future maritime Ground Based Augmentation Systems". In: *Proceedings of the* 2^{nd} *GNSS Vulnerabilities and Solutions Conference*. Baska, Croatia.

Parkinson, Bradford W. and Penina Axelrad (1988). "Autonomous GPS Integrity Monitoring Using the Pseudorange Residual". In: *Navigation: Journal of The Institute of Navigation* 35.2, pp. 255–274.

Petovello, Mark G. (2002). "Real-Time Integration of a Tactical-Grade IMU and GPS for High-Accuracy Positioning and Navigation". PhD thesis. Calgary, Alberta: University of Calgary.

Ryan, Samuel J. (2002). "Augmentation of DGPS for Marine Navigation". PhD thesis. Calgary, Alberta, Canada: Department of Geomatics Engineering, University of Calgary.

Teunissen, P.J.G. (1998). "GPS for Geodesy". In: Springer. Chap. Quality control and GPS.

Thrun, Sebastian, Wolfram Burgard, and Dieter Fox (2005). *Probabilistic Robotics (Intelligent Robotics and Autonomous Agents)*. The MIT Press. ISBN: 0262201623.

Walter, Todd, Todd Walter, and Per Enge (1995). *Weighted RAIM for Precision Approach*.

Wang, Jian-Guo (2008). "Test Statistics in Kalman Filtering". In: *Journal of Global Positioning Systems* 7.1, pp. 81–90.

Wieser, A. and F. Brunner (2000). "An extended weight model for GPS phase observations". In: *Earth Planet Space* 52, pp. 777–782.

Ziebold, Ralf, Zhen Dai, Thoralf Noack, and Evelin Engler (2010). "Concept for an integrated PNT-unit for maritime applications". In: *Satellite Navigation Technologies and European Workshop on GNSS Signals and Signal Processing (NAVITEC), 2010 5th ESA Workshop on*, pp. 1–8.